Metal Ion-Induced Lateral Aggregation of Filamentous Viruses fd and M13

Jay X. Tang,* Paul A. Janmey,† Alexander Lyubartsev,‡ and Lars Nordenskiöld‡

*Physics Department, Indiana University, Bloomington, Indiana 47405, †Institute for Medicine and Engineering and Departments of Physiology and Physics and Astronomy, University of Pennsylvania, Philadelphia, Pennsylvania 19104 USA, and ‡Physical Chemistry, Arrhenius Laboratory, Stockholm University, S-10691 Stockholm, Sweden

ABSTRACT We report a detailed comparison between calculations of inter-filament interactions based on Monte-Carlo simulations and experimental features of lateral aggregation of bacteriophages fd and M13 induced by a number of divalent metal ions. The general findings are consistent with the polyelectrolyte nature of the virus filaments and confirm that the solution electrostatics account for most of the experimental features observed. One particularly interesting discovery is resolubilization for bundles of either fd or M13 viruses when the concentration of the bundle-inducing metal ion Mg^{2+} or Ca^{2+} is increased to large (>100 mM) values. In the range of Mg^{2+} or Ca^{2+} concentrations where large bundles of the virus filaments are formed, the optimal attractive interaction energy between the virus filaments is estimated to be on the order of 0.01 kT per net charge on the virus surface when a recent analytical prediction to the experimentally defined conditions of resolubilization is applied. We also observed qualitatively distinct behavior between the alkali-earth metal ions and the divalent transition metal ions in their action on the charged viruses. The understanding of metal ions-induced reversible aggregation based on solution electrostatics may lead to potential applications in molecular biology and medicine.

INTRODUCTION

Many filamentous biopolymers such as DNA and protein filaments are highly charged polyelectrolytes that frequently occur in compact and ordered forms in biological systems (Alberts et al., 1994). The common findings of lateral association between these negatively charged filaments suggest a general explanation based on solution electrostatics (Pelta et al., 1996; Tang and Janmey, 1996; Tang et al., 1996; Gelbart et al., 2000; Lyubartsev and Nordenskiöld, 2002). Recently, much attention has been focused on theoretical predictions of the attractive interaction between like-charged cylindrical polyelectrolytes in an aqueous medium, which is induced by multivalent counterions (Ray and Manning, 1994; Lyubartsev and Nordenskiöld, 1995; Tang et al., 1996; Rouzina and Bloomfield, 1996, 1997; Gronbech-Jensen et al., 1997; Ha and Liu, 1997, 1998; Lyubartsev et al., 1998; Shklovskii, 1999a,b; Gelbart et al., 2000; Nguyen et al., 2000a,b,c; Nguyen and Shklovskii, 2001a,b).

Several approaches attempt to predict the interfilament interactions between charged rodlike polyelectrolytes (Philip and Wooding, 1970; Dewey, 1990; Rajasekaran and Jayaram, 1994; Ray and Manning, 1994; Lyubartsev and Nordenskiöld, 1995; Sharp, 1995; Sharp et al., 1995; Stigter, 1995; Rouzina and Bloomfield, 1996, 1997; Gronbech-Jensen et al., 1997; Ha and Liu, 1997, 1998; Lyubartsev et al., 1998; Shklovskii, 1999a,b; Nguyen et al., 2000b,c; Nguyen and Shklovskii, 2001a,b). The first step of most theoretical analyses is the Poisson–Boltzman equation. It has been well recognized, however, that no attractive interactions can be produced based on the mean-field Poisson–Boltzman treatment unless some correlation between counterions is introduced (Le Bret and Zimm, 1984; Guldbrand et al., 1986; Anderson and Record, 1990; Nilsson et al., 1991; Lamm et al., 1994; Gronbech-Jensen et al., 1997; Gelbart et al., 2000). As first noted by Kirkwood and Schumaker (1952) and treated by Oosawa (1971) using an approximate analytical treatment, the net force between two adjacent polyions might become attractive due to the correlated fluctuations in the ion clouds surrounding them. Thus, when the average distance between two filaments of like charge is large in comparison with the diameter of small ions, filament–filament attraction is related to the correlation of thermal fluctuations of the screening atmospheres formed by the small ions. At smaller distances, the Manning (1978) condensation of ions on the surface of charged rods may lead to strong spatial correlations of ions (Rouzina and Bloomfield, 1996; Shklovskii, 1999a; Nguyen et al., 2000a) or even the formation of Wigner crystals (Gronbech-Jensen et al., 1997; Shklovskii, 1999b). Independent of these analytical treatments, an electrostatic attraction for rodlike polyelectrolytes has also been demonstrated using Monte Carlo (MC) simulations for a system of hexagonally ordered rodlike polyelectrolytes such as DNA (Guldbrand et al., 1986; Nilsson et al., 1991) and filamentous phages (Lyubartsev et al., 1998).

The long-standing interest in the mechanism of attractive interaction for cylindrical polyelectrolytes has largely been motivated by an attempt to understand the formation of densely packed DNA that occurs upon addition of multiva-

Submitted December 20, 2001 and accepted for publication March 20, 2002.

Lars Nordenskiöld's current address is the School of Biological Sciences, Nanyang Technological University, Singapore 637616.

Address reprint requests to Jay X. Tang, Physics Department, Indiana Univ., Swain West 165, 727 East Third St., Bloomington, IN 47405. Tel.: 812-855-6857; Fax: 812-855-5533; E-mail: jxtang@indiana.edu.

0006-3495/02/07/566/16 $2.00

lent counterions, a phenomenon known as DNA condensation (Manning, 1978; Baeza et al., 1987; Arscott et al., 1990; Bloomfield, 1991; Marquet and Houssier, 1991; Ma and Bloomfield, 1994; Gelbart et al., 2000). Recently, a number of other negatively charged rodlike biopolymers such as F-actin and filamentous bacteriophages have been shown to form laterally ordered aggregates, or bundles, due to the presence of divalent and multivalent cations, some of which are their natural counterions (Tang and Janmey, 1996; Tang et al., 1996, 1997).

Filamentous bacteriophages provide an ideal set of test systems for the effect of electrostatics on the lateral association of highly charged rodlike polyelectrolytes. Two closely related bacteriophages fd and M13, for example, are long and stiff rodlike particles with identical size but different surface charge density (Lyubartsev et al., 1998). Each virus is coated by approximately 2700 copies of polypeptide that cover the interior single-stranded, circular DNA, giving the virion a length of 880 nm and a diameter of 6.6 nm (Makowski, 1984; Day et al., 1988; Model and Russel, 1988; Tang and Fraden, 1995). The persistence length of both viruses is greater than 2 μm, allowing for the approximation of them as straight rods, whereas the electrostatic interaction between neighboring filaments is the focus of consideration. M13 and fd differ by a single amino acid in their major coat-protein subunit, a 50-amino acid helical polypeptide (Day et al., 1988). As a result of this difference, M13 has one negative charge less per subunit than fd, corresponding to a 25–30% reduction in surface charge density. The protein assembly of the virus particles is known to near atomic resolution (Makowski, 1984) and the intact viruses are structurally stable in solution over a wide range of ionic conditions (Tang and Fraden, 1995). Therefore, we use these viruses as a model system for testing theoretical predictions of interactions between rodlike polyelectrolytes.

Present analytical predictions of attractive interactions are successful only at the qualitative level due to a number of simplifying assumptions. Specifically, most analytical treatments have not taken into consideration the finite size of counterions and co-ions in solution. Such parameters, along with the size and distribution of individual ions on the macroions, can be considered in computer simulations (Lyubartsev et al., 1998). We present in this paper a detailed survey of lateral aggregation of fd and M13 viruses induced by a number of divalent metal ions. The experimental data are compared with the results of grand canonical MC simulations taking into explicit consideration parameters such as ion size and surface charge distribution of the virus particles.

Our experimental findings are consistent with predictions based on MC simulations in several aspects. First, divalent cations such as Ca^{2+} and Mg^{2+} mediate sufficient attractive interaction to cause lateral aggregation of both fd and M13 and the concentrations experimentally required agree with predictions of the onset of attraction based on computer simulations within a factor of two. Second, the MC simulations correctly predict that the divalent cation-induced attractive interaction is stronger for the more highly charged fd viruses, which require a lower concentration of the cations to form lateral aggregates. Third, the prediction that counterions of larger diameter are less capable of mediating attractive forces is supported by the experimental data, considering hydrated ion size. Fourth, monovalent salt competitively interacts with the charged filaments and acts to reduce the attractive interaction mediated by the divalent cations.

There are also two novel findings of our experimental study that are not directly accounted for by the predictions of the computer simulations. First, we experimentally detected solubilization of the virus bundles with excess divalent cations on the order of a hundred millimolar. A more explicit term of resolubilization is used throughout the paper to describe the two-step phenomenon that the viruses initially dispersed in solution first form precipitating aggregates and then disperse back to solution by increasing the concentration of divalent counterions. The computer simulations using an effective hydrated ion diameter yield increasing attraction, whereas the opposite trend is required to predict the experimentally observed resolubilization behavior for the virus bundles. However, on the basis of additional simulations using a naked ion diameter, which display a decrease in attraction between the viruses as a function of increasing divalent salt in the bulk, we obtain support for the notion that effects on the ion hydration are important for the resolubilization phenomenon. Second, we found distinct features of bundle formation by divalent transition metal ions including an opposite trend in threshold concentrations required to bundle fd and M13 and no resolubilization after bundles were formed. The possibility of specific interactions between the ions and the virus surface is discussed in addition to the general electrostatics.

MATERIALS AND METHODS

Preparation of fd and M13 viruses

The fd and M13 phages were both prepared by a standard method (Sambrook et al., 1989). Freeze-dried fd and M13 and their host *Escherichia coli* bacteria (strain K38) were purchased from the American Type Culture Collection (Manassas, VA). A large amount of the progeny phages were separated from the bacterial media by multiple steps of sedimentation and resuspension, followed by a final separation step using the cesium-chloride density-gradient method. The virus suspensions were kept in a low ionic-strength buffer containing 2 mM HEPES, pH 7.5, and 1 mM NaN_3.

Electron microscopy

Electron micrographs were obtained with a JEOL 1200-EX transmission electron microscope using 1% uranyl acetate for staining (Tang et al., 1996). The specimens were viewed and photographed at 100 kV and 50,000× magnification.

Dynamic light scattering

Dynamic light scattering was performed with a Brookhaven Instruments (Holtsville, NY) device consisting of a 10-mW He-Ne laser, a BI-160 goniometer, a photomultiplier connected to a BI-2030AT correlator, and a computer to control the measurement settings and analyze the scattering data (Janmey et al., 1994). The total scattering events and the intensity autocorrelation counts were collected at the 90° scattering angle.

Electrophoresis

Agarose gel electrophoresis was used to measure the migration of intact viruses under an electric field. Aliquots of fd and M13 solutions were loaded into small wells cast in a 0.8% agarose gel. The intact viruses were then subjected to a constant electric field, and the distances of migration were measured and compared. Instead of using ethidium bromide to label the polynucleotide within the core of the viruses, we used Coomassie blue to stain the protein coat after electrophoresis, which allowed convenient viewing under visible light.

Static light scattering

Measurements of light scattering intensity at the 90° angle were performed with a Perkin-Elmer LS-5B luminescence spectrometer (Tang and Janmey, 1996; Tang et al., 1996). The incident wavelength was set to 365 nm (3-nm slit) and the scattered light was detected at 375 nm (3-nm slit) to reduce the signal level. A rectangular light-scattering cuvette of 10-mm path length and 5-mm width held 600 μl of typically a 0.1 mg/ml virus solution. The initial scattering intensities for the solutions of both fd and M13 viruses were the same within experimental variation. Each subsequent reading represents a scattering intensity measured when the solution reached a steady state following an addition of a stock solution of concentrated $MeCl_2$, where Me represents any of the divalent metal ion species.

Optical microscopy

Large bundles of viruses were observed by means of a Nikon TE-300 microscope under the phase contrast mode with a 60× oil objective. The images were taken using a Sanyo CCD camera with a 1.5× coupler. The dimension of the optical field was calibrated using an optical micrometer.

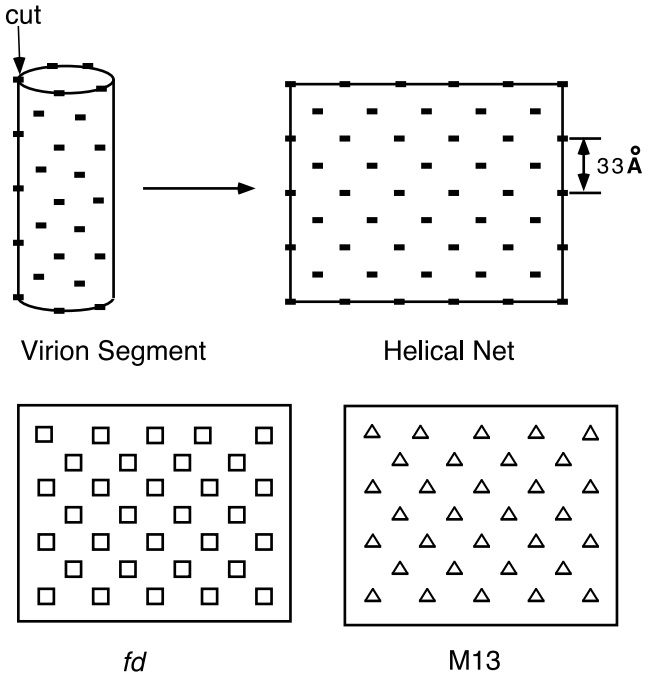

FIGURE 1 Schematics of the surface charge positions for the filamentous phages fd and M13. *Top Left*, Positions of the protein subunits on a segment of fd/M13 virus. *Top Right*, Helical net of the virion, viewed by cutting and unfolding the cylindrical surface. One negative charge is positioned at every corner of the small squares for fd (*bottom left*) or triangles for M13 (*bottom right*). All objects are drawn to scale as indicated on the top right.

MONTE CARLO SIMULATIONS

Monte Carlo simulations were performed for a model system consisting of an infinite array of hexagonally packed polyelectrolyte rods separated by a variable distance r (distance between the polyion surfaces) with mobile ions between them. The fd and M13 virions and the electrostatic interactions have been modeled in the following way, as depicted in Fig. 1 (Lyubartsev et al., 1998). The rods are treated as infinitely long hard cylinders of diameter 6.0 nm and with discrete negative charges at the surface of the rod. Four negative elemental charges are assigned to represent the effective net surface charge for each fd coat-protein subunit. The positions of the four charges form a square of 10 Å on each side, and the centers of such squares are placed at the surface of the cylinder so that their positions are consistent with the crystallographic packing of the subunits (Makowski, 1984). The only difference in the treatment of the M13 virion is that each subunit is assigned three negative elemental charges placed to form a unilateral triangle. This arrangement gives average axial linear charge separations of $b = 0.825$ Å and 1.1 Å for fd and M13, respectively. The solvent water is treated as a dielectric continuum described by a dielectric permitivity $\epsilon = 78$ at close to ambient temperature ($T = 300$ K). The mobile ions and the rod charges are described as point charges $q_i = z_i e$, with a repulsive r^{-12} potential of effective hydrated diameter d_i. The value of d_i is set to 4 Å for the negative charges on the rod and for the monovalent mobile ions of either sign. The diameter d_i for the divalent ions can be varied, and this is then a way to take into account not just the bare diameter of the counterions, but also the effects of the solvent water on the effective hydration of the multivalent ions in an averaged form. The total potential energy of the system (excluding the hard rod term) is

$$U = \sum_{i<j} \frac{q_i q_j}{4\pi\epsilon_0\epsilon r_{ij}} + kT \sum_{i<j} \left(\frac{d_i + d_j}{2r_{ij}}\right)^{12}, \qquad (1)$$

where $r_{ij} = r_i - r_j$ is the distance between ions i and j.

The calculations have been performed in a simulation "box" with the shape of a hexagonal prism containing one rod and of height $h = 9.9$ nm and side length L, defined by the given variable rod–rod separation r, $L = (r + a)/\sqrt{3}$,

where a is the diameter of the rod. Periodic boundary conditions were applied in all directions, thus modeling an infinite lattice of hexagonally ordered rods. The long-range electrostatic interactions from the lattice of surrounding cells were included as in the previous work using the Ewald summation method (Lyubartsev and Nordenskïold, 1995).

In the experiments, the well-defined salt concentration of the bulk is in equilibrium with that of the ordered (bundled) phase, whereas the salt content of the bundles is unknown and determined by the condition of equilibrium between the phases. Therefore, the MC simulations have been performed within the grand canonical ensemble under the condition of equal chemical potential in the phases obtained from separate simulations of the bulk electrolyte solution (Lyubartsev and Nordenskïold, 1995). The effective force between the ordered rods is directly related to the osmotic pressure in the rod system. The quantity of interest is the relative osmotic pressure P_{osm} for a given separation between the rods,

$$P_{osm} = P_{rod}(r) - P_{bulk}. \quad (2)$$

Here, $P_{rod}(r)$ is the pressure of the ordered rod phase at separation r, and P_{bulk} is the pressure of the bulk phase. The pressure can be evaluated based on its thermodynamic relationship as the derivative of the corresponding free energy with respect to volume V. Within the grand canonical ensemble, the pressure in either of the two systems ($P_{rod}(r)$ or P_{bulk}) is thus given by

$$P = kT \left. \frac{\partial \ln(\Xi)}{\partial V} \right|_{T,\mu}. \quad (3)$$

Here, Ξ is the grand canonical partition function, and μ is the chemical potential of the system. The right-hand side of Eq. 3, which is related to the free energy derivative of the system, has been evaluated using the expanded ensemble method (Lyubartsev and Nordenskiöld, 1995). Within this method, the ratio of partition functions at different distances r is obtained by varying r within the MC procedure with biased potential and calculating probability distributions over r. Other details of the procedure have been published previously (Lyubartsev and Nordenskiöld, 1995).

In the simulations, the bulk has been modeled as a mixture of 2:1 and 1:1 salt, MeX_2/MX, where $z_{Me} = +2$, $z_X = -1$ and $z_M = +1$. The concentration of divalent salt has been varied while the monovalent salt is kept constant at 2 mM. This is chosen to conform to the experiments where the bulk consists of divalent salt $MeCl_2$ (where Me = Ca or Mg), as well as ~2 mM monovalent ions in the buffer.

RESULTS

The results of this work are organized into three parts. In the first subsection, we characterize the closely related fd and M13 viruses using three experimental techniques to establish their suitability for this study. In the next subsection, theoretical predictions from MC simulations are presented with a group of six figures. The simulations results include osmotic pressure curves for a number of conditions and distributions of both counterions and co-ions at close to the rod surface with the presumed hexagonal packing. Major experimental results are presented in the third subsection. Features of the reversible bundle formation were measured by static light scattering. The onset bundling threshold concentrations are summarized in Table 1 for a total of six species of divalent metal ions. In addition to results based on the light scattering detection, morphological characteristics of the virus bundles measured by optical microscopy are compared at selected conditions.

The selection of fd and M13 viruses as model systems

To confirm the structural similarity and the quality of the virus preparations used in our study, fd and M13 viruses were imaged by electron microscopy using the widely-used negative staining method. Fig. 2 compares the two viruses under the same preparation conditions. The filament length of fd is slightly larger than M13 by only a few percent, which is comparable to the experimental error. The fd filaments appear to be surrounded by more staining materials visible by close comparison of Fig. 2, *A* and *B*. This slight difference between the electron micrograph images is likely because fd particles are more negatively charged and thus attract more uranium ions used for the staining procedure. Aside from this difference, which varied depending on the electron micrograph preparation, the two viruses appear to be nearly identical in size and shape.

We further test whether the point mutation on each of the major coat proteins of M13 alters their packing on the virion enough to alter filament stiffness using dynamic light scattering, a technique that has been used to measure the persistence length of many filamentous biopolymers, including fd and M13 (Loh et al., 1979; Maeda and Fujime, 1985; Song et al., 1991) and the cytoskeletal protein filaments F-actin (Janmey et al., 1994). Fig. 3 shows identical curves for the normalized intensity autocorrelation function, strongly suggesting that the two viruses display the same stiffness in solution under thermal undulations. These measurements are also consistent with previous light-scattering studies performed by different laboratories, which obtained the same persistence length of 2.2 μm for fd and M13 (Loh et al., 1979; Maeda and Fujime, 1985; Song et al., 1991).

One clear difference between the two viruses is that an M13 virus is expected to carry ~30% less surface charge than fd based on the biochemical analysis. The only difference between fd and M13 at the genetic level is a point mutation in the gene VIII, which expresses ~2700 copies of the major coat protein subunits. As a consequence, the aspartic acid residue of fd at position 12 from the N-terminal end is replaced by asparagine for M13 (Model and

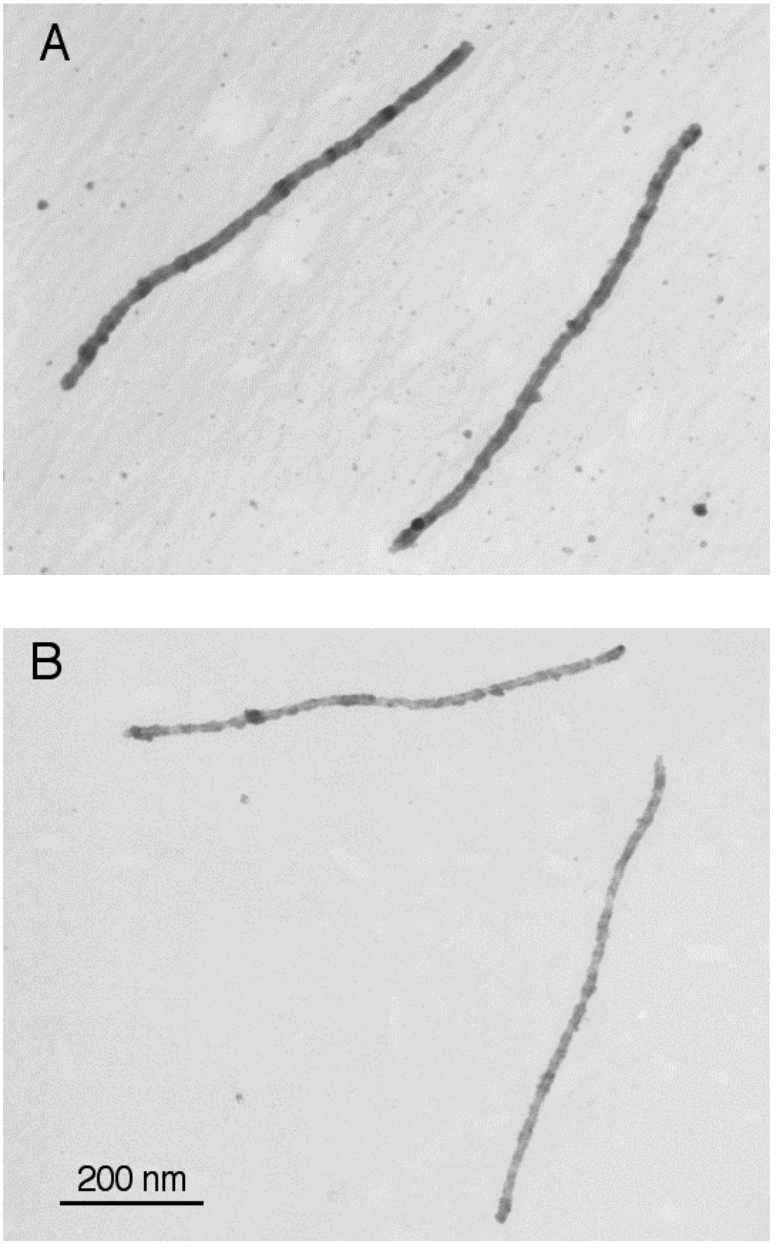

FIGURE 2 Electron micrographs of (*A*) fd and (*B*) M13 viruses. Both images were taken with the same magnification. The viruses were prepared under the same negative staining procedure as described in the Materials and Methods section.

Russel, 1988). Position 12 is exposed at the viral surface in proximity with four other negative residues and one positively charged lysine at the end of the subunit exposed to the solvent. Therefore, M13 is expected to carry approximately ¼ less surface charge at near neutral pH. The exact ratio of the surface-charge density is expected to vary as a function of pH. We confirm this prediction at pH 7.5 by electrophoresis (Fig. 4). The ratio of the travel distances between the two viruses is determined to be 0.73:1 (M13:fd), which is close to the predicted ratio of their surface-charge densities based on the molecular composition of the viruses. Note that such an agreement is only approximately true for the two viruses of identical sign and shape and under the restricted experimental condition that only monovalent counterions are present. A detailed electrophoretic study of fd and M13 viruses with the presence of divalent counterions forms the subject of a separate ongoing study.

Monte Carlo simulations results

Osmotic pressure was calculated for two surface-charge distributions, as described in the Monte Carlo Simulations section, to mimic that of fd and M13. For both viruses, the pressure curves are repulsive at low concentrations of divalent cations. At increasing divalent counterion concentrations, the pressure becomes less repulsive at intermediate distances (~10 Å). Above a threshold concentration of the

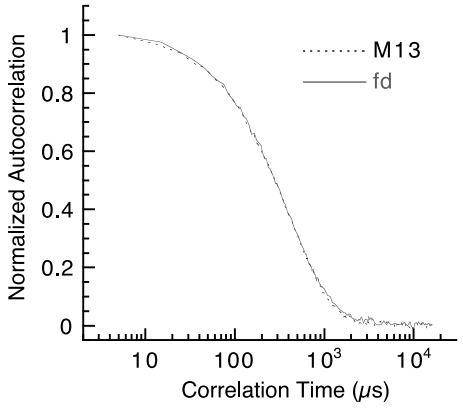

FIGURE 3 Intensity autocorrelation function of fd and M13 viruses. The data were collected using a dynamic light-scattering setup. The complete overlap between two autocorrelation profiles suggests that the thin filaments of the two types of viruses have most likely identical length, diameter, and persistence length.

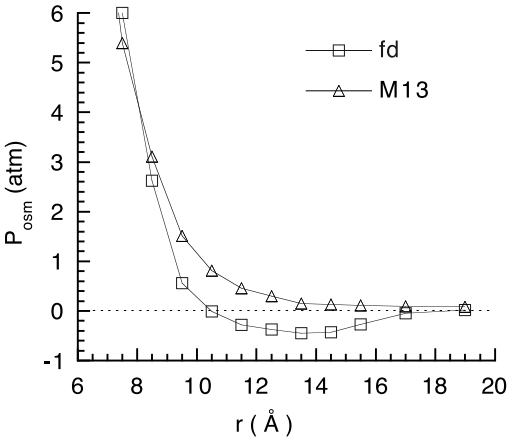

FIGURE 5 The calculated osmotic pressure P_{osm}, as a function of rod–rod surface separation r, for an array of hexagonally packed fd or M13 viruses. The simulations were performed for 50 mM divalent salt (MeX_2) with diameter d_{Me} = 5 Å. A fixed ion diameter of 4 Å was used for all monovalent ions throughout the simulations.

divalent salt, an attractive minimum is shown at ~11 Å spacing. As shown in our preceding publication (Lyubartsev et al., 1998), the attractive force appears when the concentration [MeX_2] in the bulk is larger than 25 mM for the case of the fd virus. Additional increases of the divalent salt give more pronounced levels of attraction. For M13, the onset of attraction starts at a significantly higher concentration of ~70 mM divalent cations.

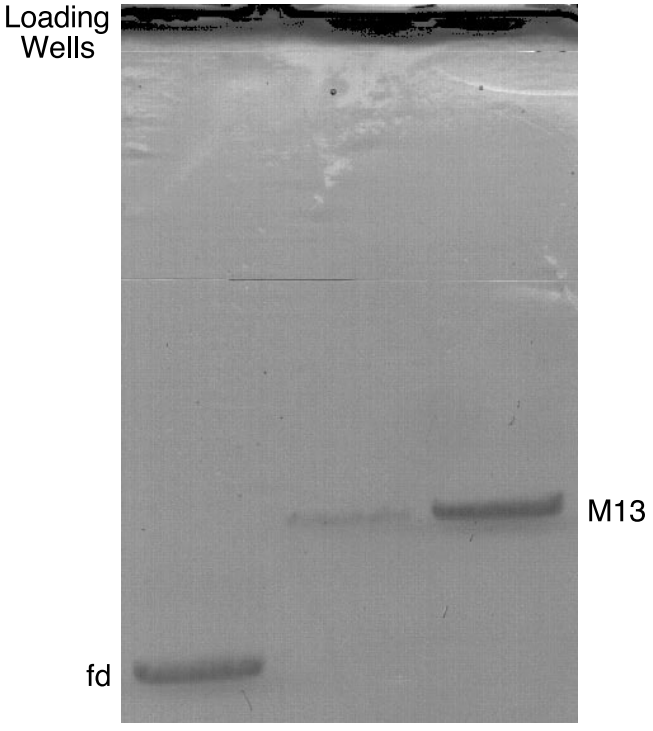

FIGURE 4 Agarose gel electrophoresis of fd and M13 viruses. The ratio of migration distance of the M13 viruses to the fd viruses is measured to be 0.73. The viruses have identical size, and their mobility is found to be proportional to their net surface charge as predicted by their molecular composition.

Figure 5 shows a close comparison between the pressure curves of fd and M13 with the divalent cation concentration set at 50 mM with ionic diameter of 5 Å. For the more highly charged fd viruses, the osmotic pressure becomes negative when the distance between the hexagonally packed filaments of higher charge is in the range of 11–16 Å. This result suggests spontaneous formation of bundles. The pressure curve remains positive for the less charged M13 under the same ionic conditions, suggesting no lateral aggregation at this condition.

To evaluate the effect of the hydrated counterion diameter on lateral interaction between the highly charged fd filaments, osmotic pressure was calculated from the simulations with ion diameters of 4, 5, and 6 Å, respectively, taking 35 mM as the concentration of divalent salt. A monotonic reduction of the negative pressure region is seen in Fig. 6 as the ionic radius is increased. At a diameter of 6 Å or above, the pressure curve remains positive through the entire range of spacing, suggesting that no aggregation occurs with counterions so large. Our simulations predict that the onset of negative pressure is displaced from ~25 mM divalent salt to ~50 mM when increasing the divalent ion diameter from 5 to 6 Å. A similar effect is observed for M13, in which case the divalent ion concentration for onset negative pressure is increased from ~70 mM to 100 mM.

Solutions of biological polyelectrolytes often contain a complex mixture of salts. Because monovalent salt is expected to interfere with the association of divalent counterions with the polyelectrolyte, MC simulations were performed for a fixed concentration of 100 mM Me^{2+} of diameter 5 Å with various concentrations of monovalent salt. The set of four curves shown in Fig. 7 shows that

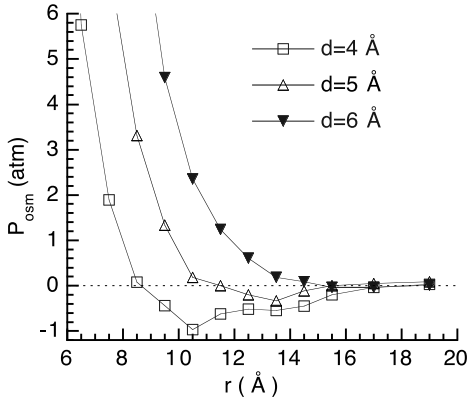

FIGURE 6 The calculated osmotic pressure P_{osm}, as a function of rod–rod surface separation r, for a large bundle of hexagonally packed fd filaments. The different curves have been calculated for 35 mM concentrations of varying diameters of the divalent counterion diameter (d_{Me} = 4, 5, and 6 Å), showing a diminishing region of negative osmotic pressure with increasing counterion diameter.

increasing the concentration of monovalent salt reduces the depth of the pressure minimum. This implies that, with an increasing amount of monovalent salt present, a larger concentration of divalent counterions is needed to induce bundling.

The calculation of pressure was extended to the extreme condition, in which hundreds of millimolar divalent metal ions are present in solution. The purpose of this calculation was to show whether a regime of resolubilization is predicted by the simple electrostatics alone. The set of four curves in Fig. 8 *A* show a deepening region of negative pressure up to 830 mM Me^{2+} with 5-Å effective hydrated ion diameter. The position of attraction minimum also shifts toward a shorter separation distance with the increasing concentration of divalent ions. It should be noted that small

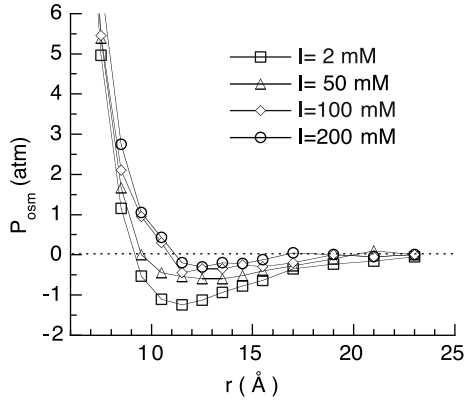

FIGURE 7 The calculated osmotic pressure P_{osm}, as a function of rod–rod surface separation r, for a large bundle of hexagonally packed fd filaments. The curves show four different concentrations of the monovalent salt, whereas the concentration of divalent counterion is fixed at 100 mM. The ion diameters are d_{2+} = 5 Å and $d_{1\pm}$ = 4 Å.

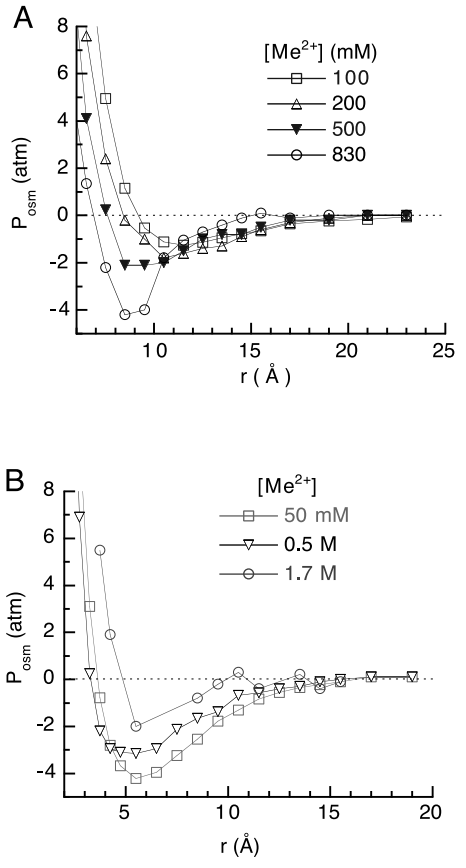

FIGURE 8 (*A*) The calculated osmotic pressure P_{osm}, as a function of rod–rod surface separation r, for a large bundle of hexagonally packed fd filaments. The different curves have been calculated for varying concentrations of divalent counterions with diameter 5 Å. A range of negative pressure is shown for all concentrations of divalent ions above a threshold, and the magnitude of attractive interaction grows with the concentration of divalent cations. (*B*) Same calculations, except with the divalent counterion diameter 1 Å. The region of negative pressure becomes narrower and shallower upon increase of the salt concentration.

kinks on the curves reflect statistical fluctuations of 0.3 atm or so, which is deemed insignificant due to the limited simulation size used. We have performed an additional simulation at 500 mM divalent salt for a system using seven polyions in the MC cell and obtained essentially the same result as for a single polyion (data not shown). As will be discussed below, the experiments actually show resolubilization of the virus bundles at high concentrations of divalent salt, which is not predicted under the conditions used in the simulations.

Additional simulations were performed to test whether the failure of the simulations to predict resolubilization is caused by the dehydration effect at high concentrations of divalent salt. At very high concentrations of divalent counterions, there are perhaps insufficient water molecules to fully hydrate all the ions, and the hydration shells of the ions may be disrupted. This would suggest that, experimentally, at very high divalent bulk salt, the effective hydration di-

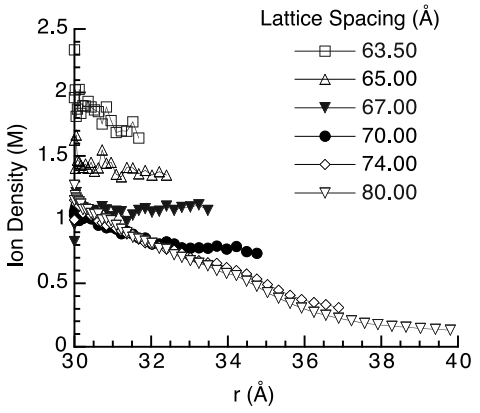

FIGURE 9 Density profile of divalent cations near fd filaments in a hexagonal lattice of several lattice spacings. The ion density is plotted up to the half lattice spacing. Note the curves appear rather flat in the $r < 35$-Å region, and the ion density near the virus surface is ~1 M when the virus filaments are larger than 7 Å apart. The bulk concentration of the simulated divalent cations is 50 mM.

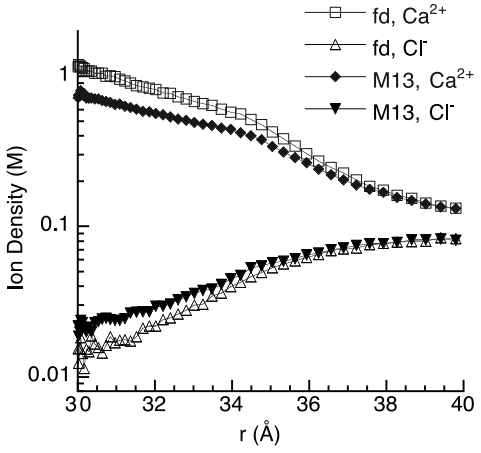

FIGURE 10 Density profiles of the divalent counterions and monovalent co-ions near the surface of fd and M13 viruses. The virus filaments are placed with the rod–rod surface spacing of 80 Å, sufficiently far away from each other for this calculation so that the ion density distribution approximates those surrounding a single filament.

ameter of all charged species is much smaller than 5 Å. To test this hypothesis, we performed a set of simulations for small ion diameters of 1 Å of all charged species in the bulk for a number of divalent salt concentrations. The results are displayed in Fig. 8 *B*. The set of three curves clearly shows a trend that the magnitude of osmotic pressure decreases at high Me^{2+} concentrations. This behavior is opposite from the case of large (5-Å) ion diameter when an increase of the divalent salt concentration leads to further increase of attraction.

One additional aspect of the simulation results is the radial distribution of counterion density. The diameter of the rod was chosen so that the center of Me^{2+} ions are 30 Å from the axis of the rod as they are in direct contact. The calculated counterion density is shown in Figs. 9 and 10 as a function of such a radial distance. Because of the presumed hexagonal packing, the calculated radial ion density data are only meaningful up to the closest hexagonal cell boundary, i.e., midpoint between the neighboring rods. Nevertheless, the simulation results for the case of fd with 50 mM Me^{2+} show that the ion density is rather flat within the $r < 35$ Å region, and the ion density near the virus surface is ~1 M when the virus filaments are larger than 7 Å apart (Fig. 9). Such a feature confirms the general prediction of counterion condensation in the sense that the counterion density does not decay exponentially near the rod surface as would be expected based on the simple Debye screening effect. Even as the charged rods are packed rather tightly, the counterion density does not reach much above 2 M, a value still significantly lower than the solubility limit. Figure 10 compares the density profiles of both the divalent counterions and monovalent co-ions near the surface of fd and M13 viruses. The virus filaments are placed with a rod–rod surface spacing of 80 Å, sufficiently far away from each other for this calculation so that the ion density distribution approximates those surrounding a single filament.

Experimental results

Bundle formation induced by divalent alkali-earth metal ions

The divalent cations of alkali-earth metal elements have complete shells of electrons and no chemical interaction with polyelectrolytes other than the nonspecific electrostatics is expected. To test the predictions of computer simulations, a series of light-scattering measurements was performed to locate and compare the threshold concentrations of these ions required to induce lateral aggregation. All four alkali-earth metal ions tested induce bundle formation of the highly charged fd viruses. The order is shown in Fig. 11 *A*, with decreasing potency in the order of $Ca^{2+} > Mg^{2+} > Ba^{2+} > Sr^{2+}$, and concentrations of 45, 65, 75, and 90 mM, respectively, required to bundle the fd viruses. The calcium ion, having the highest bundling potency in the series, is the only one capable of inducing bundle formation of the less charged M13 viruses (Fig. 11 *B*). The experimental results are qualitatively consistent with the computer simulation results showing the same trend of variation and threshold concentrations expected in the range over 25 mM divalent cations in solution. The bundling efficiency of the alkali-earth ions does not scale simply with either their crystal or hydrated ionic radii. In contrast, the hydrated radii of 4.5, 5.9, 3.7, and 3.7 Å for Ca^{2+}, Mg^{2+}, Ba^{2+}, and Sr^{2+}, respectively (Bianchi, 1968), are within the range where simulations predict that fd virus should be bundled by them. We also note that different values are given for these hydrated ion radii in a few newer references. For instance, the

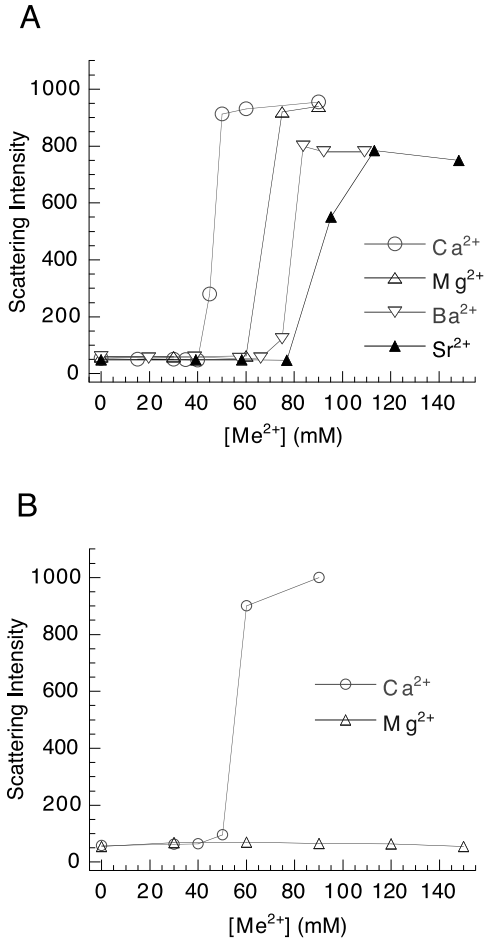

FIGURE 11 Light-scattering intensity versus concentration of added alkali-metal ions, including Ca^{2+}, Mg^{2+}, Ba^{2+}, and Sr^{2+}. (*A*) All four ions induce bundle formation of fd filaments, but (*B*) only Ca^{2+} induces bundle formation of M13 filaments. The curves for Ba^{2+} and Sr^{2+} are as flat as that for Mg^{2+} (not shown in the figure for clarity).

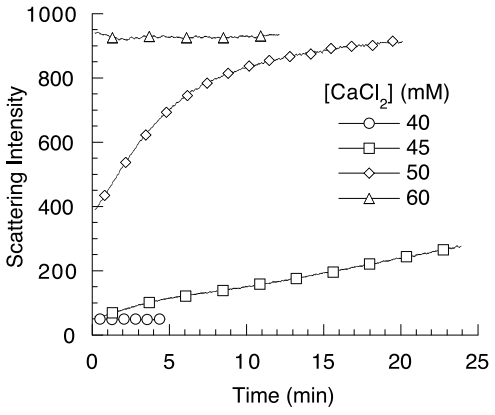

FIGURE 12 Light-scattering signal monitored following each addition of Ca^{2+}. No meaningful data were obtained within the first 2–4 s, which was required to mix the solution following each addition. Slow kinetics is noted at 45 and 50 mM Ca^{2+}, a narrow range that defines the onset bundling threshold. The final values on all four curves were plotted in the corresponding curve for the case of Ca^{2+} in Fig. 11 *A*.

hydrated ion radii of Mg^{2+} and Ca^{2+} are also listed as 5.72 and 5.39 Å, respectively (Vericat and Grigera, 1982), and 5.52 Å for Mg^{2+} (Corti and Fernandez-Prini, 1986). It appears from the existing literature that the exact radius of a hydrated metal ion remains a rather poorly defined parameter (which is perhaps why it is not tabulated in the CRC Handbook of Chemistry and Physics).

The light-scattering measurements show slow kinetics of fd aggregation near the threshold concentration of ions required for the lateral association (Fig. 12). While sequentially adding $CaCl_2$ into an fd solution, no aggregation occurred until [$CaCl_2$] was 40 mM. Addition of $CaCl_2$ to 45 mM led to a slow increase in light-scattering signal that maintained a constant rate up to 24 min. At that time, another addition of $CaCl_2$ to 50 mM markedly enhanced the speed of the aggregation to reach a plateau level on a time scale of 10 min. Further addition of $CaCl_2$ to 60 mM and beyond caused no subsequent increase of the light-scattering signal, suggesting that the virus bundles have either reached some average terminal size or grown large enough to saturate the light-scattering signal detectable at the 90° angle. When $CaCl_2$ was added to excess starting from a concentration much below the threshold, we observed immediate aggregation with a shorter time scale than a second or so required to mix the added stock solution of $CaCl_2$ with the suspension of virus particles (data not shown).

The morphology of the large virus bundles was observed by optical microscopy. Figure 13 compares bundles of fd and M13 formed by addition of 100 mM $CaCl_2$. Both types of the virus particles laterally aggregate into cylinders of contour length much larger than the length of individual viruses. The M13 bundles have shorter average length and appear to be more disordered with more branched structure, perhaps indicative of weaker attractive interactions in these bundles.

The diameter of these large bundles is rather well defined as visualized by optical microscopy. Very few much smaller bundles were seen, which would still be well within the detection limit of the microscope used. This observation was also confirmed by low-speed centrifugation under chosen conditions at which only large aggregates sediment. When large bundles were observed by microscopy, nearly all viruses sedimented into a pellet after centrifugation at $10{,}000 \times g$ for 2 min.

We estimated the average diameter of fd bundles by counting the number of virus bundles in a field of measured area under the microscope. The spread area of a 5-μl suspension of fd virus bundles was measured to cover an area of $\sim$1 cm^2. The total number of virus particles can be calculated from the concentration (typically 0.1 mg/ml) and molecular weight (16.4×10^6 for either virus). The number of virus particles per bundle is therefore equal to the number of virus particles in the sample divided by the number of

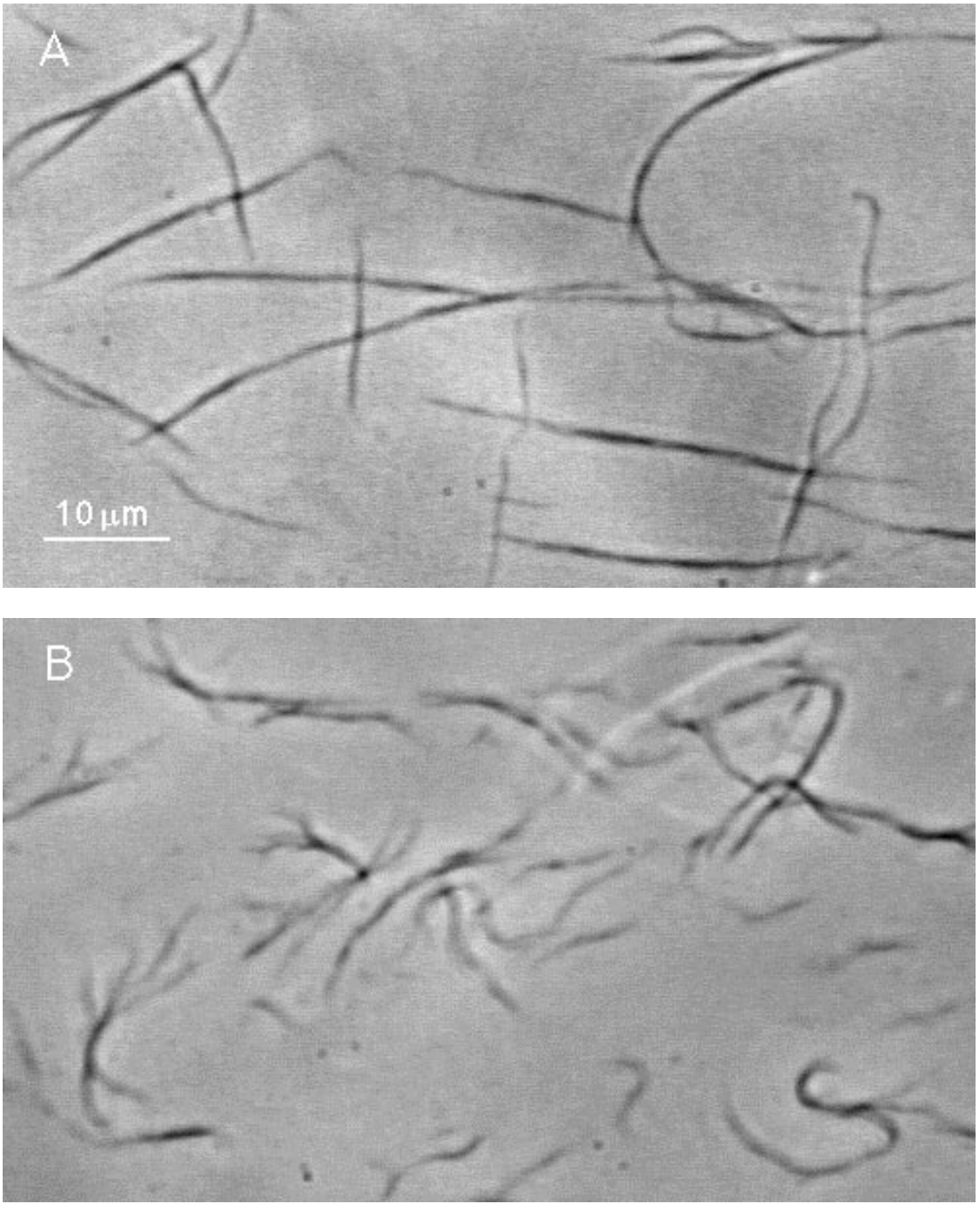

FIGURE 13 Phase contrast microscopy images of (*A*) fd and (*B*) M13 bundles, both induced by 100 mM $CaCl_2$. Each bundle was determined to contain thousands of virus filaments, and the average diameter of the tubular bundles is ~0.2 μm. M13 bundles are shorter and occasionally branch open toward the ends, indicative of weaker interfilament association.

bundles determined. This number is estimated to be $\sim 8.0 \times 10^4$ per bundle of an average length of 20 μm or so. The cross-sectional diameter is therefore estimated to be ~150 nm, assuming that the filaments are nearly close packed in the bundle. We did not attempt to estimate the average diameter of M13 bundles using this method, because the M13 bundles are shorter, more branched, more distorted, and thus harder to yield a reliable estimate.

To determine the effect of monovalent salt on bundle formation, light-scattering measurements of bundle formation were performed with 0, 50, and 100 mM KCl, respectively, before sequential additions of $CaCl_2$. The onset concentration of $CaCl_2$ required for bundling was 45, 65, and 80 mM, respectively (Fig. 14). Such experiments were performed for both viruses and with a number of divalent metal ions, and the results are shown in Table 1. These

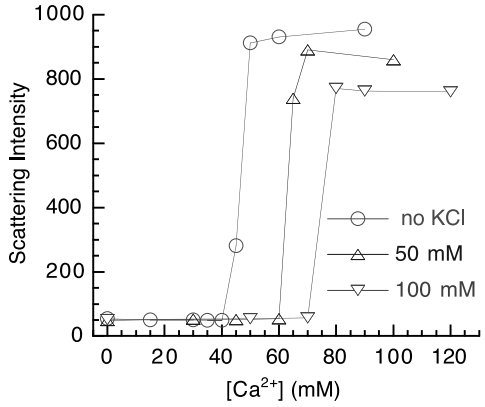

FIGURE 14 Light-scattering detection of fd bundle formation by Ca^{2+} with three KCl concentrations of 0, 50, and 100 mM. The shift of the onset bundling condition is consistent with the theoretical prediction that monovalent salt competitively reduces the bundling efficiency of the divalent counterions.

results are in agreement with the theoretical predictions of Fig. 7, which show that the attraction between fd viruses at 100-mM divalent metal ion concentration with effective hydrated ion diameter of 5 Å is reduced upon increasing the concentration of the monovalent salt. Similar results are known for the phenomenon of DNA condensation both theoretically (Manning, 1978) and experimentally (Li et al., 1998). The competition effect of monovalent salt is remarkable, especially in the case when the cationic species are weak to induce bundle formation. Presence of 100 mM KCl totally obliterated the bundle formation by Mg^{2+}, Sr^{2+}, or Ba^{2+}.

Bundles of fd and M13 were solubilized by an excess concentration of divalent metal ions such as Ca^{2+} (Fig. 15). Similar results were reported for condensed DNA using the trivalent cobalt hexamine and polyamines such as spermine and spermidine (Pelta et al., 1996). The concentration range of Ca^{2+} for resolubilization is 300–430 mM for fd and 200–290 mM for M13. Bundles of the more highly charged fd viruses require a higher concentration of $CaCl_2$ to dissolve than the less-charged M13 viruses. The range of resolubilization concentrations is nearly independent of the

TABLE 1 Threshold concentrations (in mM) of six divalent-metal ions for bundle formation of fd and M13

	fd			M13		
[KCl]	0	50	100	0	50	100
$[Mg^{2+}]$	65	90	–	–	—	—
$[Ca^{2+}]$	45	65	80	60	90	–
$[Sr^{2+}]$	100	140	–	–	—	—
$[Ba^{2+}]$	80	100	–	–	—	—
$[Mn^{2+}]$	20	27.5	35	15	30	35
$[Co^{2+}]$	10	12.5	17.5	6	13	15

–, No bundle formation up to 500 mM divalent salt added.
—, Not tested because no bundle formation is expected based on the trend.

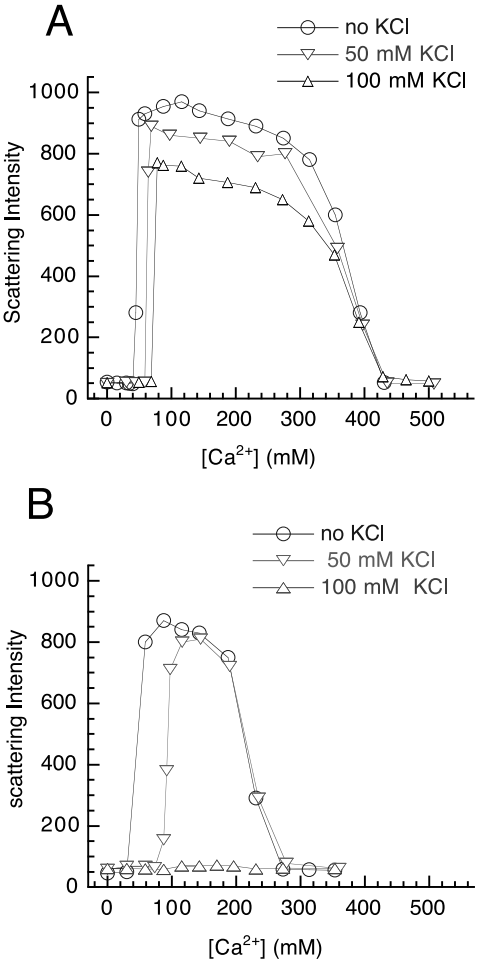

FIGURE 15 Bundle formation and subsequent solubilization following sequential additions of Ca^{2+}. The experiments are shown for both (*A*) fd and (*B*) M13, each with three concentrations of monovalent salt KCl.

monovalent salt in solution, as predicted by a recent analytical treatment (Nguyen et al., 2000c). The other alkali-earth metal ions also led to resolubilization of fd as they caused bundle formation when the monovalent salt concentrations were low (Table 1). For example, the resolubilization concentration of Mg^{2+} is about the same as that of Ca^{2+}. The resolubilization concentration of Sr^{2+} is ranged 250–300 mM, which is lower than that for Mg^{2+} and Ca^{2+}. Not only is the range of $[Sr^{2+}]$ within which fd bundles are formed narrow, but also the scattering intensity does not reach nearly as high as for the Mg^{2+}- or Ca^{2+}-induced bundles. These results suggest that Sr^{2+} is a weaker bundling cation than Mg^{2+} or Ca^{2+}.

The analytical treatment by Shklovskii and co-workers (Perel and Shklovskii, 1999; Nguyen et al. 2000c) can be applied to the data shown in Fig. 15 to estimate the concentration of Ca^{2+} at which the attractive interaction between the virus filaments in the bundles are strongest (N_0) and the interaction energy per virus surface charge (ϵ). From the fd curve without monovalent salt (Fig. 15 *A*), we take N_c

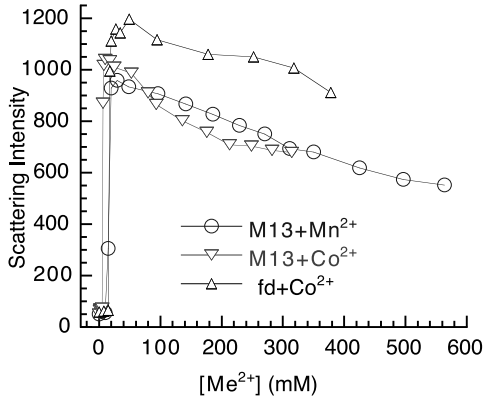

FIGURE 16 Light-scattering experiments of fd and M13 bundle formation by adding transition-metal ions Mn^{2+} and Co^{2+}. No solubilization behavior is observed, in contrast to the results shown in Fig. 15 by adding Ca^{2+}.

$= 45$ mM as the onset bundling concentration, $N_d = 400$ mM as the onset solubilization concentration, and the virus radius $a = 3.5$ nm, and follow the calculation described in the reference to obtain $N_0 = 158$ mM and $\epsilon/kT = 0.02$. Similarly, from the M13 curve without monovalent salt, we take $N_c = 60$ mM and $N_d = 280$ mM, to obtain $N_0 = 140$ mM and $\epsilon/kT = 0.013$.

Bundle formation by transition metal ions

Divalent ions of transition-metal elements interact with fd and M13 differently from the alkali-earth metal ions. First, the divalent transition-metal ions are more potent in causing bundle formation. Concentrations on the order of 10 mM are required for Mn^{2+} and Co^{2+} to bundle either fd or M13 (Table 1). These concentrations are a few-fold lower than those required for bundling by Mg^{2+} and Ca^{2+}. The concentration required for other transition-metal ions, such as Cu^{2+} or Zn^{2+}, is much lower (data not shown). The available estimates of the hydrated radii of transition-metal ions are very similar to those of alkali-earth metals. Corti and Fernandez-Prini (1986) list the ion diameters to be 5.0, 4.94, 4.92, and 4.86 Å for Mn^{2+}, Zn^{2+}, Co^{2+}, and Cu^{2+}, respectively. This suggests that a higher ability of the transition-metal ions to cause bundle formation is due to more specific metal–protein interactions. Second, the threshold concentration of either Mn^{2+} or Co^{2+} to bundle M13 viruses is lower than for fd. This trend is opposite to the case of alkali metal ions (Table 1). Third, resolubilization did not occur when excess transition-metal ions were added, but rather the light-scattering signal decreased only slightly due to the dilution effect (Fig. 16). Large aggregates persist even when the concentrations of Mn^{2+} and Co^{2+} surpass 1M (data not shown). All three features suggest a different mode of interaction between transition-metal ions/viruses and alkali-metal ions/viruses.

The morphology of both fd and M13 bundles induced by transition-metal ions is also markedly different from that of virus bundles formed by alkali-earth ions (Fig. 17, in contrast to Fig. 13). The bundles formed by 50 mM Mn^{2+} extended over 100 μm, with frequent loops intertwined in huge aggregates. Such morphology is consistent with stronger interactions among filaments within the bundles compared to those induced by alkali-earth metal ions.

DISCUSSION

A number of experimental techniques were used to characterize the divalent metal-ion-induced aggregation of bacteriophages fd and M13, which are two model cylindrical polyelectrolytes with identical size but distinct surface-charge densities. Among the findings in this study are resolubilization of virus bundles as the divalent counterion concentration is increased to large ($>$100 mM) values, a qualitatively distinct behavior between the alkali earth-metal ions and the divalent transition-metal ions in their action to induce the bundle formation, and large but well-defined finite bundle size. Very good agreement was found between the concentrations of Mg^{2+} and Ca^{2+} required to bundle both viruses, including the dependence of the threshold concentration on monovalent salt, and the MC predictions of the concentration for the onset of attraction, taking into account a realistic size and charge distribution of the viruses and the approximate diameters of the two hydrated metal ions.

The dynamic light-scattering technique has been widely used for determining particle size and diffusion coefficients of a vast variety of macromolecules in solution. For the filamentous bacteriophages fd and M13, dynamic light scattering was the primary technique used to determine the hydrodynamic diameter, the translational diffusion coefficient (Newman et al., 1977), and the persistence length of both viruses (Maeda and Fujime, 1985; Song et al., 1991). In this study, we obtained identical intensity autocorrelation profiles for fd and M13 (Fig. 3). These identical intensity autocorrelation profiles confirm the published results by different groups, giving, within $\sim$10% error, the same length, diameter, and persistence length of the two viruses. The curves in Fig. 3 also fit well the most recent theoretical predictions for the dynamic scattering of semiflexible polymers (Kroy and Frey, 2000), and a detailed analysis was performed in a separate study (Augustin, 1999).

Static light-scattering measurements provide a convenient detection of lateral aggregation, i.e., bundle formation of the filamentous viruses. Through sequential additions, the minimal concentrations required for bundling were measured for six species of divalent metal ions. To account for these experimental findings, predictions based on the MC simulations of attractive interactions are successful only at the qualitative level, dependent on a number of simplifying

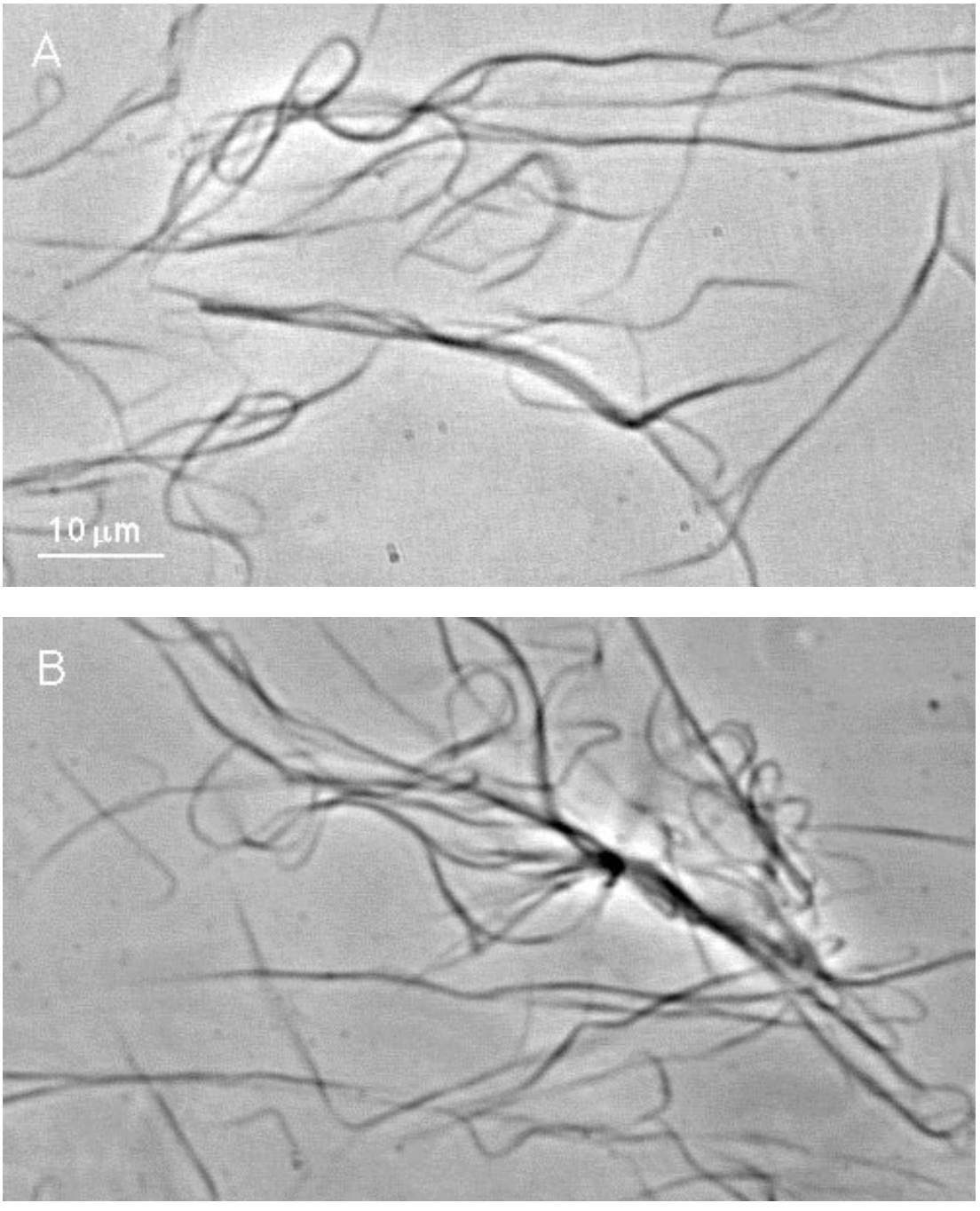

FIGURE 17 Morphology of (*A*) fd and (*B*) M13 bundles induced by 50 mM $MnCl_2$. The diameter of the tubules is comparable to the bundles induced by Ca^{2+}, as shown in Fig. 13. One distinctive feature here is that the tubular bundles surpass 100 μm in length, forming large looped and intertwined structures.

assumptions. First, water molecules are not included in the simulations, but instead, water is treated as a dielectric continuum. Second, the position of the charged residues is approximate and does not reflect the reality that these charges are at the ends of the acidic amino-acid side chains and are mobile in solution by at least several angstroms. Third, estimated values are used for the size of both the counterions in solution and the ions fixed on the viral surface. Fourth, the effect of hydration is approximated by simple adjustment of ion size.

One result of the MC simulations is the deepening of the negative pressure minimum with increasing concentration of divalent counterions using a hydrated ion diameter of 5 Å, which suggests enhanced stability of a large bundle.

However, we experimentally observed resolubilization of both fd and M13 bundles at concentrations of Ca^{2+} ions greater than a few hundred millimolar. The additional simulations performed with an ion diameter of 1 Å give results opposite to that for the hydrated ions. One possible reason for such a behavior in the case of 1-Å ion diameter is the formation of microclusters consisting of one divalent and two monovalent ions of opposite sign, a known effect in the primitive polyelectrolyte model (Weis et al., 1998). Such microclusters, although contributing to the total salt concentration, are neutral and do not contribute to the electrostatic force between the polyion. Another reason (which is actually related to the first) is a substantially higher concentration of co-ions in the ordered phase, which suppresses the fluctuation effect of divalent counterions. For example, for the 0.5-M divalent bulk salt concentration and 10-Å separation between the polyion surfaces, the average concentrations of $+2$ and -1 ions in the ordered phase were 0.34 and 0.2 M for 5-Å diameter and 0.38 and 0.3 M for 1-Å diameter, respectively. Although our data for small-ion diameter do not fully account for the resolubilization effect (the attraction does not disappear even at up to 1.7 M divalent ion concentration), they clearly show a trend in the right direction. The suggested explanations above are still incomplete. For instance, because the effective hydrated ion radius depends on the local salt concentration, it is also likely to be different between the ordered and the bulk phases. Such an effect can only be treated by explicit considerations of water molecules. Nevertheless, our data strongly suggest that the resolubilization phenomenon is likely caused by a complex interplay between pure electrostatics and the hydration effect (Rau et al., 1984; Israelachvili and Wennerstrom, 1996). A more complete theoretical treatment of this phenomenon is beyond the scope of the present work and we aim to investigate this further in a future study.

A recent analytical approach by Shklovskii and co-workers has qualitatively predicted not only the resolubilization phenomenon but also a peak value of attractive interaction (ϵ) at a defined concentration of divalent counterions (N_0) (Perel and Shklovskii, 1999; Nguyen et al., 2000c). As mentioned by these authors, their treatment is highly approximate at high concentrations of divalent salt (Perel and Shklovskii, 1999). This follows because they treat the influence of the divalent salt on the attractive force between the condensed rods using a Debye–Huckel screening. Consequently, resolubilization is always expected at high amounts of multivalent salt in the bulk due to reduction of the Debye radius. By invoking our experimental data in their analytical treatment, we estimated ϵ to be 0.02 kT for fd and 0.013 kT for M13, and N_0 to be 158 mM for fd and 140 mM for M13, all for the case of Ca^{2+}-induced bundle formation. Because each virus carries on the order of 10,000 charges on its surface, the interaction energy is on the order of 100 kT per virus in the bundled state. This value agrees well with that estimated based on the results from the MC simulations, showing a sub-atm negative pressure for over a range of a few-angstrom spacing when filaments pack to form bundles. Shklovskii and co-workers further propose that the resolubilization phenomenon is due to the reversal of surface charge (Nguyen et al., 2000c). We are currently working on testing this latest prediction of charge reversal using a number of electrophoretic techniques.

The comparison of electrostatic energy from the simulations of this report and that performed in our previous report (Lyubartsev et al., 1998) suggests that an infinitely large bundle is more electrostatically favored than small ones containing only two or three filaments. The simulation results suggest that, at the onset of counterion-induced bundling, the electrostatic interaction energy is lower for a large bundle than for many small bundles, hence the large bundles are more stable than the small ones. Such a prediction is supported by electron microscopy, which detects bundles of thousands of the virus filaments at a typical bundling condition (Tang et al., 1996). In addition, a sharp rise in light-scattering intensity by over an order of magnitude at the transition of bundle formation also suggests that, at the onset bundling condition, the lateral aggregation tends to proceed to form large bundles. However, because the formation of small bundles precedes that of larger ones, the formation of small bundles as the necessary initial step may pose a kinetic barrier for the formation of large bundles. Indeed, we observed slow light-scattering increases that took over an hour to reach stable readings within a narrow range of concentration of divalent metal ions. It is also worth noting that, due to other effects, such as a free energy barrier to add charged filaments to large existing bundles (Ha and Liu 1998) or loss of orientational entropy accompanied by the growth of large bundles (Park et al., 1998), bundles of finite final sizes may be expected and indeed are consistent with our experimental observations at the qualitative level. The kinetics and stability of the bundle formation requires consideration of many physical effects including those discussed above.

The six divalent metal ions tested in this study show no evidence for specific chemical binding to either fd or M13 virus. However, the overall trend we observed agrees quite well with the Irving–Williams series of stability, namely $Ba < Sr < Ca < Mg < Mn < Co$ (Irving and Williams, 1948). The only notable exception in our data is that Ca^{2+} clearly induces bundle formation more potently than Mg^{2+}. The uniquely large shell of hydration an Mg ion carries is likely to account for its weaker bundling activity. This order of bundling efficiency is the same as was observed for bundling of actin filaments (Tang and Janmey, 1996). The order is also identical to that of the binding affinity of these metal ions to DNA detected by Raman spectroscopy (Duguid et al., 1993), suggesting certain common features of electrostatic origin. A recent ^{25}Mg NMR study of the weak binding of Mg^{2+} to the negatively charged protein filament

F-actin shows that the Mg ions remain hydrated as they bind, at least before bundle formation (Xian et al., 1999).

Mn^{2+} and Co^{2+} bundle the less-charged M13 viruses at lower concentrations than the more-charged fd viruses. This property is opposite to all cases of alkali earth-metal ions. In addition, the bundles induced by Mn^{2+} or Co^{2+} did not dissolve when either ion was added to large excess, another property distinct from the bundles formed by the alkali earth-metal ions. Both results suggest that perhaps weak ion-specific bonds play a dominant role in the aggregation induced by the transition-metal ions, whereas the counterion-mediated electrostatic interactions are primarily responsible for the bundle formation induced by the alkali earth-metal ions. It would be interesting to know the exact location and mode of coordination of the divalent ions inside the large bundles. This goal may be achieved in certain cases by an ongoing x-ray study (G. Wong et al., University of Illinois at Urbana–Champaign, private communication).

Although the primary goal of this work is to test the theoretical predictions of counterion-induced lateral aggregation using filamentous viruses fd and M13 as simple experimental systems, the results of our experimental study have implications of biological and medical interests as well. The well-known phenomenon of DNA condensation based on essentially the same electrostatic mechanism as tested in this paper continues to be a subject of extensive study both theoretically and experimentally, with practical relevance ranging from transcription regulation to gene delivery (Huang et al., 1999). Filamentous bacteriophages have been widely used as vectors for molecular genetics. Their aggregation properties under various solution conditions may consequently affect their infectivity and cellular transport, which are of practical concern to molecular biologists. Highly charged bacteriophages are also rather common ground-water contaminants, and removal of which, based on the concept of polyelectrolyte flocculations, is recently shown to be a very useful approach (S. Grant of University of California–Irvine, private communication). Finally, because formation of large aggregates of biopolymeric filaments including DNA, F-actin and polysacharides appears in certain cellular and physiological states, such as in human airway secretions, understanding the mechanisms of solubilization of such aggregates may lead to intervention of certain disease symptoms (Sheils et al., 1996). The quantitative study of the polyelectrolyte behavior of the simple systems of fd and M13 virus solutions performed in this work may form the groundwork for more applied studies in targeted areas, such as these briefly alluded to here.

This work was supported by National Institutes of Health grants R01 HL67286 (P.A.J. and J.X.T.) and GM56707 (P.A.J.), and by National Science Foundation DMR9988389 (J.X.T.) and DMR00–79909 (P.A.J.). L.N. and A.L. acknowledge support from the Swedish Natural Science Foundation. J.X.T. would also like to acknowledge a guest stay at the Institute of Theoretical Physics, University of California–Santa Barbara, during which period the revision of this paper was made.

REFERENCES

Alberts, B., D. Bray, J. Lewis, M. Raff, K. Roberts, and J. Watson. 1994. Molecular Biology of the Cell. Garland, New York.

Anderson, C. F., and M. T. Record, Jr. 1990. Ion distributions around DNA and other cylindrical polyions: theoretical descriptions and physical implications. *Annu. Rev. Biophys. Biophys. Chem.* 19:423–465.

Arscott, P. G., A.-Z. Li, and V. A. Bloomfield. 1990. Condensation of DNA by trivalent cations. 1. Effects of DNA length and topology on the size and shape of condensed particles. *Biopolymers.* 30:619–630.

Augustin, A. 1999. Dynamic Light Scattering Study of the Filamentous Phages fd and pf1. Master's thesis, Technical University of Munich, Munich, Germany.

Baeza, I., P. Gariglio, L. M. Rangel, P. Chavez, L. Cervantes, C. Arguello, C. Wong, and C. Montanez. 1987. Electron microscopy and biochemical properties of polyamines-compacted DNA. *Biochemistry.* 26: 6387–6392.

Bianchi, C. P., editor. 1968. Cell Calcium. Appleton-Century-Crofts, New York. 8–10.

Bloomfield V. A. 1991. Condensation of DNA by multivalent cations: considerations on mechanism. *Biopolymers.* 31:1471–1481.

Corti, J., and R. Fernandez-Prini. 1986. Cluster theory applied to aqueous (2:2) electrolytes over a wide concentration range. *J. Chem. Soc. Faraday. Trans.* 82:921–932.

Day, L. A., C. J. Marzec, S. A. Reisberg, and A. Casadevall. 1988. DNA packing in filamentous bacteriophages. *Ann. Rev. Biophys. Biophys. Chem.* 17:509–539.

Dewey, T. G. 1990. A ligand binding model of counterion condensation to finite length polyelectrolytes. *Biopolymers.* 29:1793–1799.

Duguid, J., V. A. Bloomfield, J. Benevides, and G. J. Thomas, Jr. 1993. Raman spectroscopy of DNA-metal complexes. I. Interactions and conformational effects of the divalent cations: Mg, Ca, Sr, Ba, Mn, Co, Ni, Cu, Pd, and Cd. *Biophys. J.* 65:1916–1928.

Gelbart, W. M., R. F. Bruinsma, P. A. Pincus, and V. A. Parsegian. 2000. DNA-inspired electrostatics. *Physics Today.* 53:38–44.

Gronbech-Jensen, N., R. J. Mashl, R. F. Bruinsma, and W. M. Gelbart. 1997. Counterion-induced attraction between rigid polyelectrolytes. *Phys. Rev. Lett.* 78:2477–2480.

Guldbrand, L., L. Nilsson, and L. Nordenskiöld. 1986. A Monte Carlo simulation study of electrostatic forces between hexagonally oriented DNA double helices. *J. Chem. Phys.* 85:6686–6698.

Ha, B.-Y., and A. J. Liu. 1997. Counterion-mediated attraction between two like-charged rods. *Phys. Rev. Lett.* 79:1289–1292.

Ha, B.-Y., and A. J. Liu. 1998. Effects of non-pairwise-additive interactions on bundles of rodlike polyelectrolytes. *Phys. Rev. Lett.* 81: 1011–1014.

Huang, L., M. Hung, and E. Wagner, editors. 1999. Nonviral Vectors for Gene Therapy. Academic Press, San Diego.

Irving, H., and R. J. P. Williams. 1948. Order of stability of metal complexes. *Nature.* 162:746–747.

Israelachvili, J., and H. Wennerstrom. 1996. Role of hydration and water structure in biological and colloidal interactions. *Nature.* 379:219–225.

Janmey, P. A., S. Hvidt, J. Kas, D. Lerche, A. Maggs, E. Sackmann, M. Schliwa, and T. P. Stossel. 1994. The mechanical properties of actin gels: elastic modulus and filament motions. *J. Biol. Chem.* 269: 32503–32513.

Kirkwood, J. G., and J. B. Shumaker. 1952. The influence of dipole moment fluctuations on the dielectric increment of proteins in solution. *Proc. Natl. Acad. Sci. U.S.A.* 38:863–871.

Kroy, K., and E. Frey. 2000. Dynamic scattering from semiflexible polymers. *In* Scattering in Polymeric and Colloidal Systems. W. Brown, and K. Mortensen, editors. Gordon and Breach Science Publishers, Berlin. 197–249.

Lamm, G., L. Wong, and G. R. Pack. 1994. Monte Carlo and Poisson–Boltzmann calculations of the fraction of counterions bound to DNA. *Biopolymers.* 34:227–237.

Le Bret, M., and B. H. Zimm. 1984. Distribution of counterions around a cylindrical polyelectrolyte and Manning's condensation theory. *Biopolymers.* 23:287–312.

Li, A. Z., H. Huang, X. Re, L. J. Qi, and K. A. Marx. 1998. A gel electrophoresis study of the competitive effects of monovalent counterion on the extent of divalent counterions binding to DNA. *Biophys. J.* 74:964–973.

Loh, E., E. Ralston, and V. N. Schumaker. 1979. Quasielastic light scattering from solutions of filamentous viruses. *Biopolymers.* 18: 2549–2588.

Lyubartsev, A. P., and L. Nordenskiöld. 1995. Monte Carlo simulation study of ion distribution and osmotic pressure in hexagonally oriented DNA. *J. Phys. Chem.* 99:10373–10382.

Lyubartsev, A. P., and L. Nordenskiöld. 2002. Computer simulations of polyelectrolytes. *In* Handbook of Polyelectrolytes and Their Applications, Vol. 3, Chap. 11. S. K. Tripathy, J. Kumar, and H. S. Nalwa, editors. American Scientific Publishers, Los Angeles. 309–326.

Lyubartsev, A. P., J. X. Tang, P. A. Janmey, and L. Nordenskiöld. 1998. Electrostatically induced polyelectrolyte association of rodlike virus particles. *Phys. Rev. Lett.* 81:5465–5468.

Ma, C., and V. A. Bloomfield. 1994. Condensation of supercoiled DNA induced by MnCl2. *Biophys. J.* 19:234–237.

Maeda, T., and S. Fujime. 1985. Dynamic light-scattering study of suspensions of *fd* virus: application of a theory of the light-scattering spectrum of weakly bending filaments. *Macromolecules.* 18:2430–2437.

Makowski, L. 1984. Virus structures. F. A. Jurnak, A. M. McPherson, editors. Wiley-Interscience, New York. 203–253.

Manning, G. S. 1978. The molecular theory of polyelectrolyte solutions with applications to the electrostatic properties of polynucleotides. *Q. Rev. Biophys.* 2:179–246.

Marquet, R., and C. Houssier. 1991. Thermodynamics of cation-induced DNA condensation. *J. Biomol. Struct. Dynam.* 9:159–167.

Model, P., and M. Russel. 1988. Filamentous bacteriophage. *In* The Bacteriophages. R. Calender, editor. Plenum Publishing, New York. 375–456.

Newman, J., H. L. Swinney, and L. A. Day. 1977. Hydrodynamic properties and structure of fd virus. *J. Mol. Biol.* 116:593–606.

Nguyen, T. T., A. Y. Grosberg, and B. I. Shklovskii. 2000a. Macroions in salty water with multivalent ions: giant inversion of charge. *Phys. Rev. Lett.* 85:1568–1571.

Nguyen, T. T., A. Y. Grosberg, and B. I. Shklovskii. 2000b. Screening of a charged particle by multivalent counterions in salty water: strong charge inversion. *J. Chem. Phys.* 113:1110–1125.

Nguyen, T. T., I. Rouzina, and B. I. Shklovskii. 2000c. Reentrant condensation of DNA induced by multivalent counterions. *J. Chem. Phys.* 112:2562–2568.

Nguyen, T. T., and B. I. Shklovskii. 2001a. Adsorption of charged particles on an oppositely charged surface: oscillating inversion of charge. *Phys. Rev. E.* 64:1407–1415.

Nguyen, T. T., and B. I. Shklovskii. 2001b. Overcharging of a macroion by an oppositely charged polyelectrolyte. *Physica. A.* 293:324–338.

Nilsson, L. G., L. Guldbrand, and L. Nordenskiöld. 1991. Evaluation of the electrostatic osmotic pressure in an infinite system of hexagonally oriented DNA molecules: a Monte-Carlo simulation study. *Mol. Physiol.* 72:177–192.

Oosawa, F. 1971. Polyelectrolytes. Marcel Dekker, New York. 113.

Park, S. Y., D. Harries, and W. M. Gelbart. 1998. Topological defects and the optimum size of DNA condensates. *Biophys. J.* 75:714–720.

Pelta, J., F. Livolant, and J. L. Sikorav. 1996. DNA aggregation induced by polyamines and cobalthexamine. *J. Biol. Chem.* 271:5656–5662.

Perel, V. I., and B. I. Shklovskii. 1999. Screening of a macroion by multivalent ions: a new boundary condition for the Poisson–Boltzmann equation and charge inversion. *Physica. A.* 274:446–453.

Philip, J. R., and R. A. Wooding. 1970. Solution of the Poisson–Boltzmann equation about a cylindrical particle. *J. Chem. Phys.* 52:953–959.

Rajasekaran, E., and B. Jayaram. 1994. Counterion condensation in DNA systems: the cylindrical Poisson–Boltzmann model revisited. *Biopolymers.* 34:443–445.

Rau, D. C., B. Lee, and V. A. Parsegian. 1984. Measurement of the repulsive force between polyelectrolyte molecules in ionic solution: hydration forces between parallel DNA double helices. *Proc. Natl. Acad. Sci. U.S.A.* 81:2621–2625.

Ray, J., and G. S. Manning. 1994. An attractive force between two rodlike polyions mediated by sharing of condensed counterions. *Langmuir.* 10:2450–2461.

Rouzina, I., and V. A. Bloomfield. 1996. Macroion attraction due to electrostatic correlation between screening counterions. 1. Mobile surface-adsobed ions and diffuse ion cloud. *J. Phys. Chem.* 100:9977–9989.

Rouzina, I., and V. A. Bloomfield. 1997. Competitive electrostatic binding of charged ligands to polyelectrolytes: practical approach using the non-linear Poisson–Boltzmann equation. *Biophys. Chem.* 64:139–155.

Sambrook, J., E. F. Fritsch, and T. Maniatis. 1989. Molecular Cloning: A Laboratory Manual. Cold Spring Harbor Laboratory Press, Cold Spring Harbor, New York. 4.21–4.31.

Sharp, K. 1995. Polyelectrolyte electrostatics: salt dependence, entropic, and enthalpic contributions to free energy in the nonlinear Poisson–Boltzmann model. *Biopolymers.* 36:227–243.

Sharp, K. A., R. A. Friedman, V. Misra, J. Hecht, and B. Honig. 1995. Salt effects on polyelectrolyte-ligand binding: comparison of Poisson–Boltzmann, and limiting law/counterion binding models. *Biopolymers.* 36:245–262.

Sheils, C. A., J. Kas, W. Travassos, P. G. Allen, P. A. Janmey, M. E. Wohl, and T. P. Stossel. 1996. Actin filaments mediate DNA fiber formation in chronic inflammatory airway disease. *Am. J. Pathol.* 148:919–927.

Shklovskii, B. I. 1999a. Screening of a macroion by multivalent ions: correlation-induced inversion of charge. *Phys. Rev. E.* 60:5802–5811.

Shklovskii, B. I. 1999b. Wigner crystal model of counterion induced bundle formation of rodlike polyelectrolytes. *Phys. Rev. Lett.* 82: 3268–3271.

Song, L., U.-S. Kim, J. Wilcoxon, and J. M. Schurr. 1991. Dynamic light scattering from weakly bending rods: estimation of the dynamic bending rigidity of the M13 virus. *Biopolymers.* 31:547–567.

Stigter, D. 1995. Evaluation of the counterion condensation theory of polyelectrolytes. *Biophys. J.* 69:380–388.

Tang, J. X., and S. Fraden. 1995. Isotropic-cholesteric phase transition in colloidal suspension of filamentous bacteriophage fd. *Liquid Crystals.* 19:459–467.

Tang, J. X., T. Ito, T. Tao, P. Traub, and P. A. Janmey. 1997. Opposite effects of electrostatics and steric exclusion on bundle formation by F-actin and other filamentous polyelectrolytes. *Biochemistry.* 36: 12600–12607.

Tang, J. X., and P. A. Janmey. 1996. Polyelectrolyte nature of F-actin and mechanism of actin bundle formation. *J. Biol. Chem.* 271:8556–8563.

Tang, J. X., S. Wong, P. T. Tran, and P. A. Janmey. 1996. Counterion induced bundle formation of rodlike polyelectrolytes. *Ber. Bunsen-ges Phys. Chem.* 100:796–806.

Vericat, F., and J. R. Grigera. 1982. Theoretical single-ion activity of calcium and magnesium ions in aqueous electrolyte mixtures. *J. Phys. Chem.* 86:1030–1032.

Weis, J. J., D. Levesque, and J. M. Caillol. 1998. Restricted primitive model of an ionic solution confined to a plane. *J. Chem. Phys.* 109: 7486–7497.

Xian, W., J. X. Tang, P. A. Janmey, and W. H. Braunlin. 1999. The polyelectrolyte behavior of actin filaments: a 25Mg NMR study. *Biochemistry.* 38:7219–7226.